


Thermodynamic consideration and ground-state search of icosahedral boron subselenide $B_{12}(B_{1-x}Se_x)_2$ from a first-principles cluster expansion

A. Ektarawong*

Theoretical Physics Division, Department of Physics, Chemistry and Biology (IFM), Linköping University, SE-581 83 Linköping, Sweden
 (Received 5 March 2018; revised manuscript received 27 April 2018; published 11 May 2018)

The phase stability of icosahedral boron subselenide $B_{12}(B_{1-x}Se_x)_2$, where $0.5 \leq x \leq 1$, is explored using a first-principles cluster expansion. The results show that, instead of a continuous solid solution, $B_{12}(B_{1-x}Se_x)_2$ is thermodynamically stable as an individual line compound at the composition of $B_{9.5}Se$. The ground-state configuration of $B_{9.5}Se$ is represented by a mixture of $B_{12}(Se-Se)$, $B_{12}(B-Se)$, and $B_{12}(Se-B)$ with a ratio of 1:1:1, where they form a periodic $ABCABC\dots$ stacking sequence of $B_{12}(Se-Se)$, $B_{12}(B-Se)$, and $B_{12}(Se-B)$ layers along the c axis of the hexagonal conventional unit cell. The structural and electronic properties of the ground-state $B_{9.5}Se$ are also derived and discussed. By comparing the derived ground-state properties of $B_{9.5}Se$ to the existing experimental data of boron subselenide $B_{\sim 13}Se$, I propose that the as-synthesized boron subselenide $B_{\sim 13}Se$, as reported in the literature, has the actual composition of $B_{9.5}Se$.

DOI: [10.1103/PhysRevB.97.174103](https://doi.org/10.1103/PhysRevB.97.174103)

I. INTRODUCTION

Icosahedral boron-rich solids have become appealing to the materials research community over the past few decades. This is attributed to their unique characteristic of the three-center two-electron chemical bonds, giving rise to several outstanding properties, e.g., high chemical and thermal stabilities, high hardness, high melting temperature, and low wear coefficient [1–8]. Together with the small atomic mass of boron, the solids also exhibit relatively low density and are thus promising candidates for a wide range of technological applications [7–16].

Among a large number of known icosahedral boron-rich solids, having been studied and reported in the literature, boron subselenide is probably the least studied. As far as I am aware, there has been only one experimental work on boron subselenide, reporting successful synthesis of the material [17]. The Rietveld analysis of the diffraction patterns obtained from x-ray powder diffraction reveals that the crystal structure of the as-synthesized boron subselenide at the claimed composition of about $B_{13}Se$ is an α -boron derivative, and the space group is $R\bar{3}m$ [17]. That is, 12-atom icosahedral clusters, composed purely of boron, are located at vertices of a rhombohedral unit cell, together with two additional atoms filling the so-called $6c$ interstitial sites between the icosahedra. Since the interstitial sites can be occupied either by selenium or by boron [17], the formula of icosahedral boron subselenide can be designated as $B_{12}(B_{1-x}Se_x)_2$. The substitution of boron for selenium at the interstices subsequently gives rise to interesting but unanswered questions, concerning stable compositions of $B_{12}(B_{1-x}Se_x)_2$ and their favored atomic configurations of B and Se atoms, in particular at the $6c$ interstitial sites.

In the present work, I aim to address the above questions, related to boron subselenide. I implement the cluster expansion

method combined with first-principles calculations in order to search for energetically stable compositions of $B_{12}(B_{1-x}Se_x)_2$ and relevant atomic configurations. The calculated results suggest that, instead of a continuous solid solution, $B_{12}(B_{1-x}Se_x)_2$ is an individual line compound, thermodynamically stable at the composition of $B_{9.5}Se$. In addition, the predicted ground state, order-disorder transition, and some intrinsic properties of $B_{9.5}Se$ are reported and compared with the existing experimental data of icosahedral boron subselenide [17] to validate the presently theoretical predictions. Also, the predicted ground state of $B_{9.5}Se$ is expected to serve as a starting configuration for further theoretical investigation—for example, atomistic modeling of brittle failure and amorphization in $B_{9.5}Se$ using the *ab initio* molecular-dynamics (AIMD) simulations, as previously carried out for icosahedral boron carbide (B_4C) [18–20].

II. METHODOLOGY

A. First-principles calculations

The first-principles total energies of all configurations of the $B_{12}(B_{1-x}Se_x)_2$ alloy, considered in the present work, are calculated from the density functional theory (DFT), where the projector augmented wave (PAW) method [21] as implemented in the Vienna *ab initio* simulation package (VASP) [22,23], and the generalized gradient approximation (GGA) proposed by Perdew, Burke, and Ernzerhof (PBE96) [24] for the exchange-correlation functional, are used. I employ the $9 \times 9 \times 9$ Monkhorst-Pack \mathbf{k} -points mesh [25] for sampling of the Brillouin zone, while the energy cutoff for plane waves, included in the expansion of wave functions, is set to 500 eV. I also assure that the calculated total energies are converged within an accuracy of 1 meV/at with respect to both the number of \mathbf{k} points and the energy cutoff. Note that, during the total energy calculations, the internal atomic coordinates, volume, and cell shape of $B_{12}(B_{1-x}Se_x)_2$ are fully relaxed. The

*annop.ektarawong@liu.se

electronic density of states of $B_{12}(B_{1-x}Se_x)_2$ is calculated via the tetrahedron method for the Brillouin zone integrations [26].

B. Cluster expansion method

Following the cluster-expansion (CE) formalism proposed by Sanchez *et al.* [27], any quantity that is strictly a function of the atomic arrangement on a lattice, generally referred to as a *configuration*—for example, the energy E —can be formally expanded into a sum over correlation functions ξ ;

$$E^{\text{CE}}(\sigma) = N \sum_{\alpha} m_{\alpha}^{(n)} V_{\alpha}^{(n)} \xi_{\alpha}^{(n)}(\sigma). \quad (1)$$

$E^{\text{CE}}(\sigma)$ is the total energy for a given configuration σ . $\xi_{\alpha}^{(n)}(\sigma)$ is the n -site correlation function of a specific figure α , defined for configuration σ . The factor $m_{\alpha}^{(n)}$ corresponds to the multiplicity of figure α , normalized to the number of sites N within configuration σ , and $V_{\alpha}^{(n)}$ is defined as the effective cluster interaction (ECI) of figure α . To describe the atomic configuration σ of icosahedral boron subselenide, the spin variable σ_i is assigned to take on a value of $+1$ or -1 if the lattice site i is occupied by a boron or selenium atom, respectively. Thus, the atomic configuration σ of boron subselenide can be uniquely specified by a set of spin variables $\{\sigma_i\}$. The n -site correlation function $\xi_{\alpha}^{(n)}$ of figure α can then be determined by the products of the spin variables σ_i ;

$$\xi_{\alpha}^{(n)} = \frac{1}{m_{\alpha}^{(n)}} \sum_{f \in \alpha} \left(\prod_{i=1}^n \sigma_i \right), \quad (2)$$

where the sum of the products in the parentheses runs over all symmetrically equivalent clusters, $f \in \alpha$. Even though the expansion, expressed in Eq. (1), is analytically exact in the limit of inclusion of all possible clusters, it must be truncated for all practical purposes.

In the present work, the cluster expansion method is performed by the MIT Ab initio Phase Stability (MAPS) code [28], as implemented in the Alloy-Theoretic Automated Toolkit (ATAT) [29], to truncate the expansion in Eq. (1) and to determine the effective cluster interactions. The interactions are determined in such a way that Eq. (1) returns the total energies as close to those obtained from first-principles calculations as possible for σ included in the expansion. Implementation of the cluster expansion to search for the ground states of $B_{12}(B_{1-x}Se_x)_2$ will be further described and discussed in Sec. III D.

III. RESULT AND DISCUSSION

A. Initial B-Se convex hull

As a first step, I consider the thermodynamic stability of two icosahedral boron subselenides at compositions of $B_{13}Se$ and B_6Se , respectively, represented in the rhombohedral primitive unit cell of 14 atoms by $B_{12}(Se-B)$ and $B_{12}(Se-Se)$, as shown in Fig. 1. B_{12} stands for the icosahedral cluster, while “-” in the parentheses denotes a vacancy residing between the two 6c interstitial atoms. The former composition is inspired by the experimental work of Bolmgren and Lundström [17], reporting successful synthesis of icosahedral boron subselenide of the claimed composition of about $B_{13}Se$. The latter composition

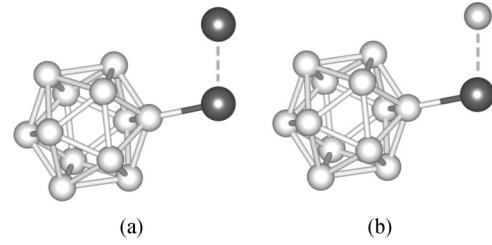


FIG. 1. Structural units of boron subselenides: (a) $B_{12}(Se-Se)$ and (b) $B_{12}(Se-B)$, corresponding to B_6Se and $B_{13}Se$ compositions, respectively. White and gray spheres represent B and Se atoms, respectively.

is, on the other hand, motivated by the idealized stoichiometry of boron suboxide (B_6O), which is also the icosahedral boron-chalcogen compound similar to boron subselenide and represented by $B_{12}(O-O)$ [30,31]. Figure 2 illustrates the formation energy (ΔE^{form}) of $B_{12}(Se-B)$ as well as $B_{12}(Se-Se)$, determined with respect to their pure elemental phases, i.e., α -boron and gray selenium. As a complement in demonstrating the stability of the two icosahedral boron subselenides, I also consider BSe_2 , found to be a stable compound for the binary B-Se system [32]. As can be seen from Fig. 2, the two icosahedral phases at the compositions of $B_{13}Se$ and B_6Se and BSe_2 form an initial B-Se convex hull, indicating their phase stability at 0 K.

B. Structural defects in the dilute limit of $B_{12}(Se-Se)$ and $B_{12}(Se-B)$

In addition to the idealized configuration of $B_{13}Se$ and B_6Se , given by an individual $B_{12}(Se-B)$ and $B_{12}(Se-Se)$, respectively, I look into the possibility for them to configurationally disorder, induced by high concentrations of structural defects: for

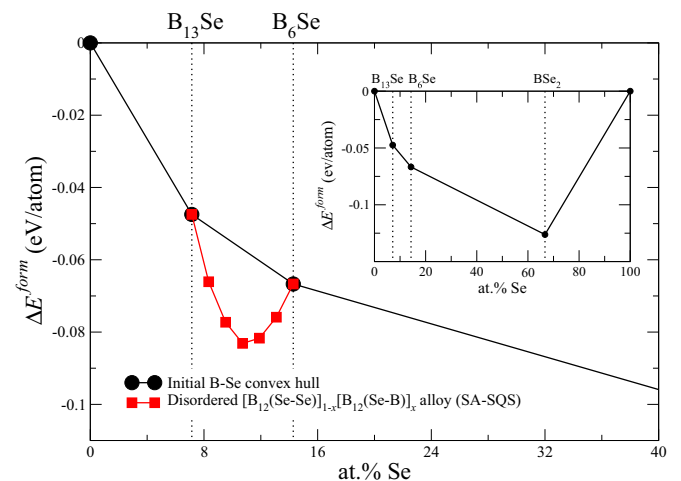


FIG. 2. Formation energy (ΔE^{form}) of boron selenides, calculated with respect to their pure elemental phases. A set of black lines, connecting filled black circles at $B_{13}Se$, B_6Se , and BSe_2 , illustrates an initially sketched B-Se convex hull. A set of red lines, connecting filled red squares, indicates ΔE^{form} of pseudobinary disordered alloys of $[B_{12}(Se-Se)]_{1-x}[B_{12}(Se-B)]_x$, modeled from the SA-SQS approach. The inset shows a full picture of the initial convex hull at 0 K.

example, (i) B/Se substitutional defects within the icosahedra and/or at the $6c$ interstitial sites, and (ii) Se and/or B vacancies at the $6c$ interstitial sites. In this section, I study different kinds of structural defects in the dilute limit, typically involved with only one or two atoms of boron and/or selenium, in the fully relaxed $2 \times 2 \times 2$ rhombohedral primitive unit cells (112 atoms) of $B_{12}(\text{Se-B})$ and of $B_{12}(\text{Se-Se})$.

I observe that the defective structures, of which (i) B substitutes for Se at one of the $6c$ interstitial sites in the matrix of $B_{12}(\text{Se-Se})$, and (ii) Se substitutes for B at one of the $6c$ interstitial sites in the matrix of $B_{12}(\text{Se-B})$, are relatively stable with respect to nondefective $B_{12}(\text{Se-B})$ and $B_{12}(\text{Se-Se})$, indicated by their ΔE^{form} lying below the *initial* convex hull (*not shown*). On the other hand, ΔE^{form} of defective structures, where (i) Se substitutes for icosahedral B, or (ii) B and/or Se at the $6c$ interstitial sites are removed to form vacancies, or (iii) B substitutes for Se at the $6c$ sites to form a B-B interstitial unit, are found to be relatively high, and they are distinctly lying above the *initial* B-Se convex hull (*not shown*). These findings are in line with the Rietveld structural analysis of x-ray diffraction patterns of boron subselenide [17], which shows that there is no substitution of Se for B occurring within the icosahedra.

C. Thermodynamics of mixing for a pseudobinary $[B_{12}(\text{Se-Se})]_{1-x}[B_{12}(\text{Se-B})]_x$ solid solution

The results, observed from the dilute defect study, also indicate a tendency of mixing between $B_{12}(\text{Se-B})$ and $B_{12}(\text{Se-Se})$ units. To examine the hypothesis, I construct structural models of disordered $B_{12}(B_{1-x}Se_x)_2$ alloys, given by $[B_{12}(\text{Se-Se})]_{1-x}[B_{12}(\text{Se-B})]_x$ within $3 \times 3 \times 2$ rhombohedral primitive unit cells (252 atoms), where $x = \frac{1}{6}, \frac{1}{3}, \frac{1}{2}, \frac{2}{3},$ and $\frac{5}{6}$, by using the superatom-special quasirandom structure (SA-SQS) approach [33–35]. For this particular case, two superatomic species, as shown in Fig. 1, are defined for modeling the alloy. As can be seen from ΔE^{form} evaluated at 0 K in Fig. 2, the pseudobinary $[B_{12}(\text{Se-Se})]_{1-x}[B_{12}(\text{Se-B})]_x$ alloy is relatively stable with respect to its constituents, that is, $B_{12}(\text{Se-B})$ and $B_{12}(\text{Se-Se})$, over a whole composition range considered. This indicates that $B_{12}(\text{Se-B})$ and $B_{12}(\text{Se-Se})$ readily mix with each other even at 0 K.

Although the obtained results clearly confirm the tendency of mixing between $B_{12}(\text{Se-B})$ and $B_{12}(\text{Se-Se})$ units, the ground-state configurations of the $B_{12}(B_{1-x}Se_x)_2$ alloy at a given composition x , needed for revision of the B-Se convex hull, are currently unknown. Apart from the substitution of Se atoms for B atoms at the $6c$ sites in the matrix of $B_{12}(\text{Se-B})$, I find that replacing a unit of Se-B by B-Se in the matrix of $B_{12}(\text{Se-B})$ does lower the total energy of boron subselenide at the global composition of $B_{13}\text{Se}$ by 22 meV. Such swapping of B and Se atoms at the $6c$ interstitial sites can thus be considered as a favorable defect for $B_{12}(\text{Se-B})$, and it must also be taken into account when searching for ground-state configurations of the $B_{12}(B_{1-x}Se_x)_2$ alloy in the following section.

D. Ground-state search of the $B_{12}(B_{1-x}Se_x)_2$ alloy

In the present section, I employ the cluster expansion method, as implemented in the ATAT package [28,29], to search

for ground-state configurations of the $B_{12}(B_{1-x}Se_x)_2$ alloy. First, I establish a database of different configurations σ of $B_{12}(B_{1-x}Se_x)_2$ using an algorithm developed by Hart and Forcade [36]. It has been shown in the previous section that no substitution of Se for B takes place within the icosahedra. One can thus presumably exclude the icosahedral atoms from the cluster expansion procedure, leaving them as spectators, and only those residing at the $6c$ interstitial sites will be considered in the cluster expansion. In addition, I have found that the substitution of B for Se at the $6c$ sites of $B_{12}(\text{Se-B})$ to form a B-B interstitial unit is very unlikely for $B_{12}(B_{1-x}Se_x)_2$. Taking into account such findings, I limit the composition of the $B_{12}(B_{1-x}Se_x)_2$ alloy to $0.5 \leq x \leq 1$, corresponding to the designation of $B_{13}\text{Se}$ to $B_6\text{Se}$.

In this particular case, I generate a set of 5764 configurations of $B_{12}(B_{1-x}Se_x)_2$ up to a supercell size of 84 atoms. The first few hundred generated configurations, whose total energies are already calculated from the first-principles approach, are chosen and included in the cluster expansion to extract ECIs up to four-body interactions. The *initial* ECIs (or Hamiltonian) obtained from the expansion of those input configurations are then used to predict the total energy of all generated configurations via Eq. (1) to search for the ground-state configurations.

The *initial* Hamiltonian may not do the prediction accurately, and thus it needs to be improved. To this end, a few hundred more low-energy configurations, predicted by the *initial* Hamiltonian, are singled out, their total energies are calculated using the first-principles approach, and they are included in the cluster expansion to rebuild the Hamiltonian. This procedure can be iterated until the cluster expansion of the total energy of the $B_{12}(B_{1-x}Se_x)_2$ alloy is converged. The final fit includes 1141 configurations of $B_{12}(B_{1-x}Se_x)_2$ in the cluster expansion, and the Hamiltonian employs a total of 82 ECIs. Apart from the zero-body and one-body interactions, the Hamiltonian is composed of 40 two-body interactions, 20 three-body interactions, and 20 four-body interactions. The final Hamiltonian fits the 1141 input configurations with the cross-validation score of 7.71 meV/site. The error distribution of the fit can be seen from Fig. 3(a), where the formation energy (ΔE) of the 1141 input configurations, as computed by first-principles DFT and the CE method, is shown.

Figure 3(b) illustrates the ground-state diagram at 0 K of icosahedral $B_{12}(B_{1-x}Se_x)_2$, where $0.5 \leq x \leq 1$. As can be seen from Fig. 3(b), the final Hamiltonian predicts, among the 5764 generated configurations, seven ground-state configurations at $x = \frac{1}{2}, \frac{2}{3}, \frac{3}{4}, \frac{4}{5}, \frac{5}{6}, \frac{11}{12},$ and 1. In addition, among the configuration of known DFT-calculated energy, the DFT-derived and CE-predicted ground states agree with each other, confirming the predictive power of the Hamiltonian.

E. Revision of the B-Se convex hull and ground-state configuration of $B_{9.5}\text{Se}$

The prediction of the ground states for the $B_{12}(B_{1-x}Se_x)_2$ alloy in the previous section subsequently results in a revision of the *initial* B-Se convex hull, as proposed in Sec. III A. The *revised* convex hull at 0 K, taking into consideration the predicted ground-state configurations of the $B_{12}(B_{1-x}Se_x)_2$ alloy, is shown in Fig. 4. As can be seen from Fig. 4 and its inset,

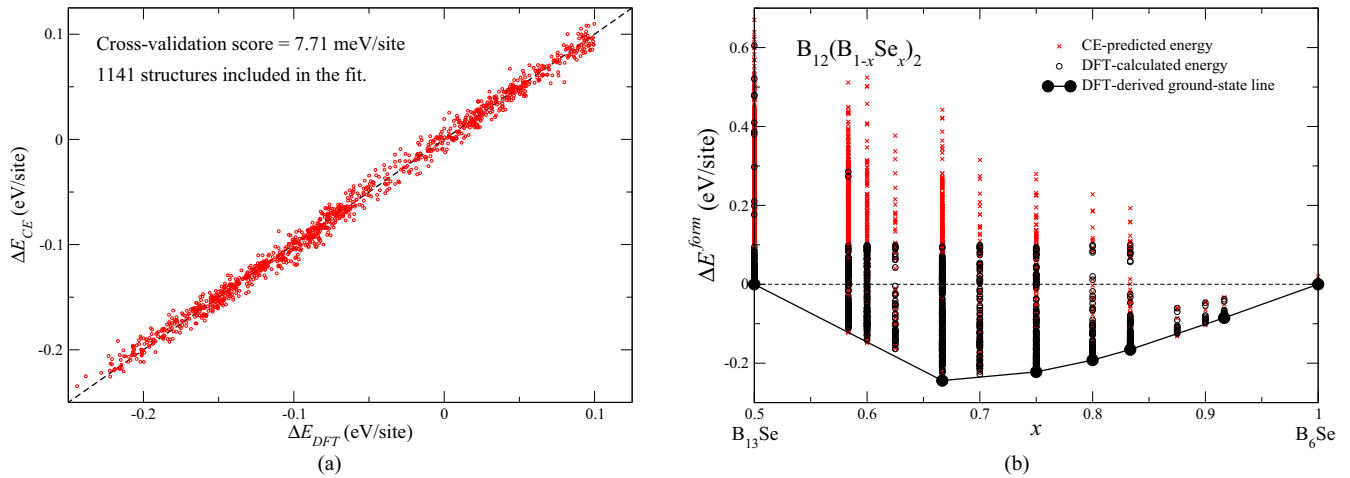


FIG. 3. (a) Formation energies ΔE of the 1141 input configurations $\{\sigma\}$, calculated from density functional theory (DFT) and predicted by the cluster expansion (CE) method using Eq. (1). The cross-validation score for the Hamiltonian, obtained from the final fit of the 1141 input configurations, is 7.71 meV/site. (b) Ground-state diagram at 0 K of icosahedral $B_{12}(B_{1-x}Se_x)_2$, where $0.5 \leq x \leq 1$. Red crosses are CE-predicted formation energy ΔE^{form} of 5764 configurations up to a supercell size of 84 atoms. Open black circles are DFT-calculated ΔE^{form} of 1141 configurations, included in the cluster expansion. The black thick line represents the DFT-derived ground-state (GS) line of $B_{12}(B_{1-x}Se_x)_2$ alloy, where the seven ground-state configurations found are denoted by large filled black circles.

only BSe_2 and the ordered configuration of boron subselenide at the composition of $B_{9.5}Se$ or $B_{12}(B_{0.33}Se_{0.67})_2$ are lying on the *revised* convex hull, thus confirming their phase stability at 0 K. On the other hand, the ordered configurations of icosahedral boron subselenide at the compositions ranging from $B_{13}Se$ to B_6Se , except that at $B_{9.5}Se$, as well as the disordered SA-SQS configurations of the $B_{12}(B_{1-x}Se_x)_2$ alloy, given by $[B_{12}(Se-Se)]_{1-x}[B_{12}(Se-B)]_x$, are clearly above the convex

hull, indicating their phase decomposition at 0 K into the relevant competing phases, i.e., α -boron, the ordered ground state of $B_{9.5}Se$ and BSe_2 , through minimizing their formation energy under the condition of thermodynamic equilibrium. It is also worth noting that the impact of lattice vibrations is completely neglected in the present work.

The ground-state atomic configuration of $B_{9.5}Se$ can be seen as a periodic stacking sequence of type $ABCABC\dots$ along the c axis of the hexagonal conventional unit cell of icosahedral boron subselenide (Fig. 5), where A , B , and C denote a layer of $B_{12}(Se-Se)$, $B_{12}(B-Se)$, and $B_{12}(Se-B)$, respectively. The configuration of $B_{9.5}Se$ can thus be written as $[B_{12}(Se-Se)]_{0.34}[B_{12}(B-Se)]_{0.33}[B_{12}(Se-B)]_{0.33}$. The optimized a and c lattice parameters of the ground state of $B_{9.5}Se$ are 5.9815 Å and 11.958 Å, respectively. These values are found to be very close to the experimental lattice parameters of icosahedral boron subselenide of the claimed composition of $B_{\sim 13}Se$, where the values of a and c are 5.9041 and 11.947

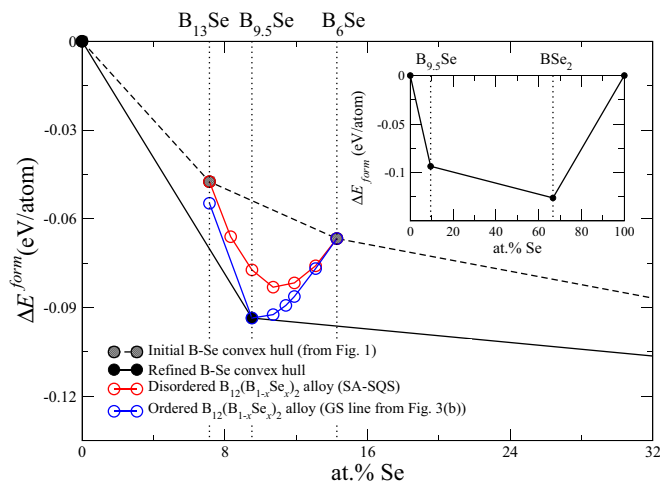


FIG. 4. Refined B-Se convex hull (black solid lines, connecting filled black circles), illustrating $B_{9.5}Se$ as a stable composition of icosahedral boron subselenide. The initial B-Se convex hull, illustrated in Fig. 1 (black dashed lines, connecting shaded black circles), is given for comparison purposes. Blue open circles represent the ordered ground-state configurations of $B_{12}(B_{1-x}Se_x)_2$ alloy, identified in Fig. 3(b), while red open circles denote the disordered SA-SQS configurations of $B_{12}(B_{1-x}Se_x)_2$ alloy, given by $[B_{12}(Se-Se)]_{1-x}[B_{12}(Se-B)]_x$. The inset shows a full picture of the refined convex hull at 0 K.

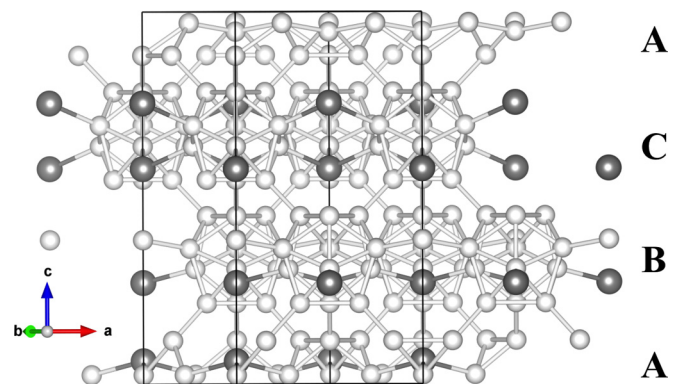


FIG. 5. Predicted ground-state configuration of $B_{9.5}Se$, given by $[B_{12}(Se-Se)]_{0.34}[B_{12}(B-Se)]_{0.33}[B_{12}(Se-B)]_{0.33}$. White and gray spheres represent B and Se atoms, respectively.

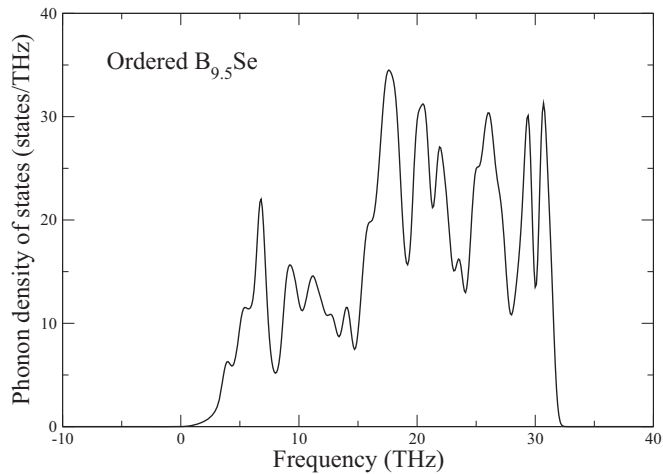


FIG. 6. Phonon density of states of the ordered $B_{9.5}Se$, given by $[B_{12}(Se-Se)]_{0.34}[B_{12}(B-Se)]_{0.33}[B_{12}(Se-B)]_{0.33}$.

Å, respectively [17]. As can be seen, the theoretical lattice parameters slightly overestimated the experimental values by less than 1.5%. By taking into account the fact that the PBE96 functional, being used in the present work, usually overestimates the equilibrium lattice parameters by approximately 1% [37], one can say that the obtained theoretical values of $B_{9.5}Se$ are in good agreement with the experiment. I thus suggest, based on the thermodynamic consideration in the present work, that the as-synthesized icosahedral boron selenide $B_{\sim 13}Se$, reported in Ref. [17], has the actual composition of $B_{9.5}Se$. A structural file in VASP format of the optimized ground-state configuration of $B_{9.5}Se$ is provided as online Supplemental Material [38].

Next, I investigate the phonon density of states of the predicted ground-state configuration of $B_{9.5}Se$ in order to inspect its dynamical stability. In this case, the phonon density of states is derived at the level of harmonic approximation by using the PHONOPY package for phonon calculations [39,40], in which the force constants are calculated within $2 \times 2 \times 1$ hexagonal conventional unit cells using the Parlinski-Li-Kawazoe method [41] with a finite displacement of 0.01 Å. By considering the phonon density of states of the ordered ground state of $B_{9.5}Se$, shown in Fig. 6, its phonon frequencies are all positive, thus confirming its dynamical stability.

It is also of interest to investigate the relative stability between ordered and disordered states of $B_{9.5}Se$, focusing on the configuration of B and Se atoms, residing at the 6c interstitial sites. To examine the configurational thermodynamics of $B_{9.5}Se$, I utilized the Hamiltonian, obtained from Sec. IIID, in canonical Monte Carlo (MC) simulations using the Easy Monte Carlo Code (EMC2) [42], as implemented in ATAT [29]. In the present work, the simulation boxes of $18 \times 18 \times 12$ rhombohedral unit cells (7776 interstitial atoms) are used. The simulations are performed within the temperature range of 50–3000 K, and the temperature step is 50 K. At each temperature, the simulations include 15 000 Monte Carlo steps (MCSs) for equilibrating the system and then 12 000 more MCSs for obtaining the proper average of the total energy as a function of temperature. The simulations reveal

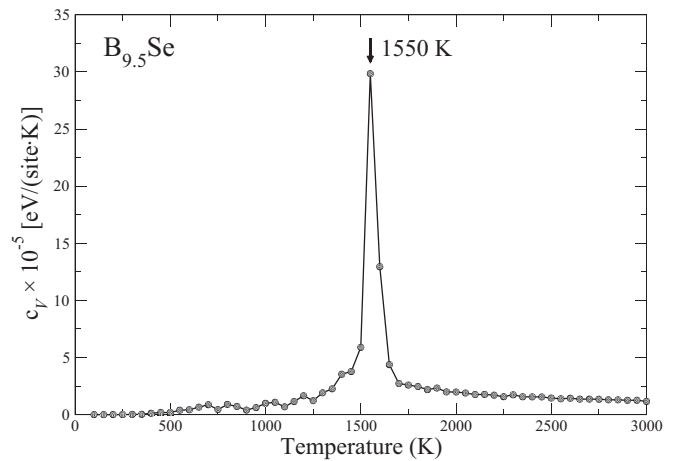


FIG. 7. Configurational specific heat (c_V) of $B_{9.5}C$ as a function of temperature evaluated from Monte Carlo simulations, using simulation boxes of $18 \times 18 \times 12$ rhombohedral unit cells.

a configurational order-disorder transition of $B_{9.5}Se$ at 1550 K as indicated by a distinct peak in the configurational specific heat (Fig. 7), derived from the obtained total energy.

F. Ground-state electronic properties of $[B_{12}(Se-Se)]_{0.34}[B_{12}(B-Se)]_{0.33}[B_{12}(Se-B)]_{0.33}$

In this section, the electronic properties of $B_{9.5}Se$, i.e., $[B_{12}(Se-Se)]_{0.34}[B_{12}(B-Se)]_{0.33}[B_{12}(Se-B)]_{0.33}$, at $T = 0$ K are provided. Figure 8(a) illustrates the electronic density of states of $B_{9.5}Se$, obtained from the use of both PBE96 and HSE06 functionals. I note that the hybrid functional HSE06 is employed in this particular case, as it is known to yield a better description of electronic band gaps for semiconductors and insulators in comparison with the semilocal PBE96 functional.

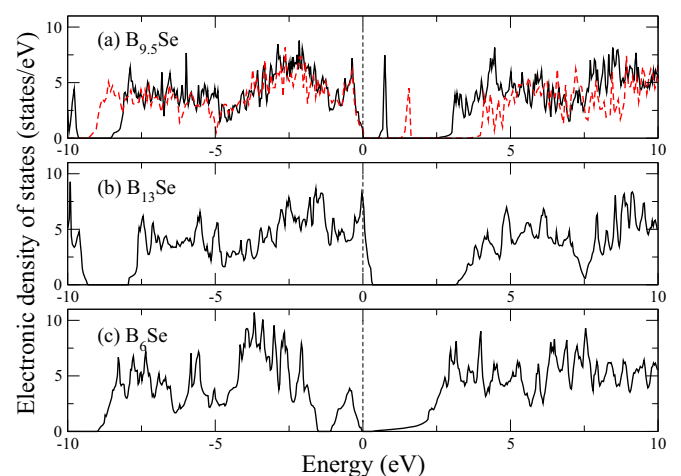


FIG. 8. Electronic density of states of (a) $B_{9.5}Se$, (b) $B_{13}Se$, and (c) B_6Se , given by $[B_{12}(Se-Se)]_{0.34}[B_{12}(B-Se)]_{0.33}[B_{12}(Se-B)]_{0.33}$, $B_{12}(Se-B)$, and $B_{12}(Se-Se)$, respectively. The black solid and red dashed lines represent the electronic density of states, obtained from the use of GGA-PBE96 and HSE06 for the exchange-correlation functional, respectively. The highest occupied state, occupied by the electrons, is indicated by the vertical dashed line at 0 eV.

This is because of the partial inclusion of the nonlocal Hartree-Fock exchange energy within the HSE06 functional. As shown in Fig. 8(a), $B_{9.5}Se$ are in both cases electrical semiconductors. The appearance of such semiconducting character of $B_{9.5}Se$ can be explained by the electron counting rules, proposed by Longuet-Higgins and Roberts [43]. According to their rules, an individual unit of $B_{12}(Se-B)$ is metallic due to the electron-deficient B_{12} icosahedral cluster, needing an extra electron to complete its bonding states. An individual unit of $B_{12}(Se-Se)$, on the other hand, is electron-precise. This is in analogy to that of icosahedral boron suboxide B_6O or $B_{12}(O-O)$, where the two oxygen atoms residing at the $6c$ interstitial sites are at the nonbonding distance [30,44]. The deficiency of an electron in $B_{12}(Se-B)$ and the electron-precise state of $B_{12}(Se-Se)$ are both confirmed by first-principles calculations and are shown, respectively, in Figs. 8(b) and 8(c).

However, in a situation in which $B_{12}(Se-Se)$ units are mixed together with $B_{12}(Se-B)$ and $B_{12}(B-Se)$ units to form the ground-state configuration of $B_{9.5}Se$ (see Fig. 5), I observe from the structural optimizations that the interatomic distance between the Se atoms residing at the $6c$ interstitial sites shrinks from the nonbonding distance of 2.945 to 2.511 Å. The shrinkage of the interatomic distance between the interstitial Se atoms results in an arrangement of diatomic chains of Se, and in turn contributes to an excess electron of two. The electron deficiency in $B_{12}(B-Se)$ and $B_{12}(Se-B)$ units can thus be compensated by the two excess electrons from the $B_{12}(Se-Se)$ unit, and the ground state of $B_{9.5}Se$, given by $[B_{12}(Se-Se)]_{0.34}[B_{12}(B-Se)]_{0.33}[B_{12}(Se-B)]_{0.33}$, behaves as a semiconductor. It is also worth noting that the ground-state configuration of $B_{9.5}Se$, predicted in the present work, is in line with the suggested electron-precise configuration of boron subselenide, based on the analysis of Bolmgren and Lundström [17]. The PBE96- and HSE06-estimated electronic band gaps of the ground-state $B_{9.5}Se$, measured from the distance between the highest occupied valence state and the lowest unoccupied midgap state, are 0.5 and 1.3 eV, respectively. Although the band gap of icosahedral boron subselenide has never been reported in experiments, the values of the band gap

of $B_{9.5}Se$, obtained in the presented work, can explain the dark brown color of the as-synthesized boron subselenide [17].

IV. CONCLUSION

I employ the first-principles cluster-expansion method to study the thermodynamic stability at 0 K of icosahedral boron subselenide $B_{12}(B_{1-x}Se_x)_2$, where $0.5 \leq x \leq 1$. The results reveal that, instead of a continuous solid solution, icosahedral boron subselenide is an individual line compound stable at the composition of $B_{9.5}Se$. The ground-state configuration of $B_{9.5}Se$ is represented by a mixture of $B_{12}(Se-Se)$, $B_{12}(B-Se)$, and $B_{12}(Se-B)$ with a ratio of 1:1:1, where they form a periodic $ABCABC\dots$ stacking sequence of $B_{12}(Se-Se)$, $B_{12}(B-Se)$, and $B_{12}(Se-B)$ layers along the c axis of the hexagonal conventional unit cell. The lattice constants of the ground state $B_{9.5}Se$ are in good agreement with the experimentally measured lattice constants of the as-synthesized boron subselenide with the claimed composition of $B_{\sim 13}Se$ [17]. Also, the electronic band gap of $B_{9.5}Se$, estimated from the hybrid functional (HSE06), is 1.3 eV. Such a band-gap value corresponds to the appearance of the dark brown pellet of the as-synthesized $B_{\sim 13}Se$ [17]. I thus suggest, based on these findings, that the as-synthesized boron selenide $B_{\sim 13}Se$ in Ref. [17] has the actual composition of $B_{9.5}Se$. To verify the proposal, further investigations of icosahedral boron subselenide are required, in particular from the experimental aspect.

ACKNOWLEDGMENTS

This research was financially supported by the Swedish Foundation for Strategic Research (SSF) through the Future Research Leaders programme (the sixth generation), granted to Björn Alling. Björn Alling is acknowledged for the fruitful discussions. All of the simulations were carried out using supercomputer resources provided by the Swedish National Infrastructure for Computing (SNIC) performed at the National Supercomputer Centre (NSC) and the Center for High Performance Computing (PDC).

-
- [1] V. Domnich, S. Reynaud, R. A. Haber, and M. Chhowalla, Boron carbide: Structure, properties, and stability under stress, *J. Am. Ceram. Soc.* **94**, 3605 (2011).
 - [2] D. Emin, Unusual properties of icosahedral boron-rich solids, *J. Solid State Chem.* **179**, 2791 (2006).
 - [3] D. Emin, Icosahedral boron-rich solids, *Phys. Today* **40**(1), 55 (1987).
 - [4] M. Carrard, D. Emin, and L. Zuppiroli, Defect clustering and self-healing of electron-irradiated boron-rich solids, *Phys. Rev. B* **51**, 11270 (1995).
 - [5] A. Hushur, M. H. Manghnani, H. Werheit, P. Dera, and Q. Williams, High-pressure phase transition makes $B_{4.3}C$ boron carbide a wide-gap semiconductor, *J. Phys.: Condens. Matter* **28**, 045403 (2016).
 - [6] S. V. Ovsyannikov, A. Polian, P. Munsch, J.-C. Chervin, G. Le Marchand, and T. L. Aselage, Raman spectroscopy of $B_{12}As_2$ and $B_{12}P_2$ up to 120 GPa: Evidence for structural distortion, *Phys. Rev. B* **81**, 140103(R) (2010).
 - [7] C. D. Frye, J. H. Edgar, I. Ohkubo, and T. Mori, Seebeck coefficient and electrical resistivity of single crystal $B_{12}As_2$ at high temperatures, *J. Phys. Soc. Jpn.* **82**, 095001 (2013).
 - [8] F. Thevénot, Boron carbide—A comprehensive review, *J. Eur. Ceram. Soc.* **6**, 205 (1990).
 - [9] M. Herrmann, I. Sigalas, M. Thiele, M. M. Müller, H. J. Kleebe, and A. Michaelis, Boron suboxide ultrahard materials, *Int. J. Refract. Met. Hard Mater.* **39**, 53 (2013).
 - [10] T. L. Aselage, D. Emin, C. Wood, I. Mackinnon, and I. Howard, Anomalous Seebeck coefficient in boron carbides, *MRS Proc.* **97**, 27 (1987).
 - [11] S. Adenwalla, P. Welsch, A. Harken, J. I. Brand, A. Sezer, and B. W. Robertson, Boron carbide/ n -silicon carbide heterojunction diodes, *Appl. Phys. Lett.* **79**, 4357 (2001).
 - [12] H. Werheit, Boron-rich solids: A chance for high-efficiency high-temperature thermoelectric energy conversion, *Mater. Sci. Eng., B* **29**, 228 (1995).

- [13] D. Emin and T. L. Aselage, A proposed boron-carbide-based solid-state neutron detector, *J. Appl. Phys.* **97**, 013529 (2005).
- [14] C. Höglund, J. Birch, K. Andersen, T. Bigault, J.-C. Buffet, J. Correa, P. van Esch, B. Guerard, R. Hall-Wilton, J. Jensen, A. Khaplanov, F. Piscitelli, C. Vettier, W. Vollenberg, and L. Hultman, B₄C thin films for neutron detection, *J. Appl. Phys.* **111**, 104908 (2012).
- [15] Y. Gong, M. Tapajna, S. Bakalova, Y. Zhang, J. H. Edgar, Y. Zhang, M. Dudley, M. Hopkins, and M. Kuball, Demonstration of boron arsenide heterojunctions: A radiation hard wide band gap semiconductor device, *Appl. Phys. Lett.* **96**, 223506 (2010).
- [16] C. E. Whiteley, Y. Zhang, Y. Gong, S. Bakalova, A. Mayo, J. H. Edgar, and M. Kuball, Semiconducting icosahedral boron arsenide crystal growth for neutron detection, *J. Cryst. Growth* **318**, 553 (2011).
- [17] H. Bolmgren and T. Lundström, The crystal structure of a new boron selenide, B₁₂Se_{2-x}B_x, *J. Alloys Compd.* **202**, 73 (1993).
- [18] X. Q. Yan, Z. Tang, L. Zhang, J. J. Guo, C. Q. Jin, Y. Zhang, T. Goto, J. W. McCauley, and M. W. Chen, Depressurization Amorphization of Single-Crystal Boron Carbide, *Phys. Rev. Lett.* **102**, 075505 (2009).
- [19] V. I. Ivashchenko and V. I. Shevchenko, First-principles study of the atomic and electronic structures of crystalline and amorphous B₄C, *Phys. Rev. B* **80**, 235208 (2009).
- [20] Q. An and W. A. Goddard III, Atomistic Origin of Brittle Failure of Boron Carbide from Large-Scale Reactive Dynamics Simulations: Suggestion Toward Improved Ductility, *Phys. Rev. Lett.* **115**, 105501 (2015).
- [21] P. E. Blöchl, Projector augmented-wave method, *Phys. Rev. B* **50**, 17953 (1994).
- [22] G. Kresse and J. Furthmüller, Efficiency of ab-initio total energy calculations for metals and semiconductors using a plane-wave basis set, *Comput. Mater. Sci.* **6**, 15 (1996).
- [23] G. Kresse and J. Furthmüller, Efficient iterative schemes for *ab initio* total-energy calculations using a plane-wave basis set, *Phys. Rev. B* **54**, 11169 (1996).
- [24] J. Perdew, K. Burke, and M. Ernzerhof, Generalized Gradient Approximation Made Simple, *Phys. Rev. Lett.* **77**, 3865 (1996).
- [25] H. J. Monkhorst and J. D. Pack, Special points for Brillouin-zone integrations, *Phys. Rev. B* **13**, 5188 (1976).
- [26] P. E. Blöchl, O. Jepsen, and O. K. Andersen, Improved tetrahedron method for Brillouin-zone integrations, *Phys. Rev. B* **49**, 16223 (1994).
- [27] J. M. Sanchez, F. Ducastelle, and D. Gratias, Generalized cluster description of multicomponent systems, *Physica A* **128**, 334 (1984).
- [28] A. van de Walle and G. Ceder, Automating first-principles phase diagram calculations, *J. Phase Equilib.* **23**, 348 (2002).
- [29] A. van de Walle, M. Asta, and G. Ceder, The alloy theoretic automated toolkit: A user guide, *CALPHAD* **26**, 539 (2002).
- [30] H. Bolmgren, T. Lundström, and S. Okada, Structure refinement of the boron suboxide B₆O by the Rietveld Method, in *Boron-rich Solids*, AIP Conf. Proc. No. 213 (AIP, New York, 1991), p. 197.
- [31] M. Kobayashi, I. Higashi, C. Brodhag, and T. Thévenot, Structure of B₆O boron-suboxide by Rietveld refinement, *J. Mater. Sci.* **28**, 2129 (1993).
- [32] H. U. Hürter, H. Eckert B. Krebs, and W. M.-Warmuth, Solid-State ¹¹B NMR studies on boron-chalcogenide system, *Inorg. Chem.* **24**, 1288 (1984).
- [33] A. Ektarawong, S. I. Simak, L. Hultman, J. Birch, and B. Alling, First-principles study of configurational disorder in B₄C using a superatom-special quasirandom structure method, *Phys. Rev. B* **90**, 024204 (2014).
- [34] A. Ektarawong, S. I. Simak, L. Hultman, J. Birch, F. Tasnádi, F. Wang, and B. Alling, Effects of configurational disorder on the elastic properties of icosahedral boron-rich alloys based on B₆O, B₁₃C₂, and B₄C, and their mixing thermodynamics, *J. Chem. Phys.* **144**, 134503 (2016).
- [35] A. Ektarawong, S. I. Simak, and B. Alling, First-principles prediction of stabilities and instabilities of compounds and alloys in the ternary B-As-P system, *Phys. Rev. B* **96**, 024202 (2017).
- [36] G. L. W. Hart and R. W. Forcade, Algorithm for generating derivative structures, *Phys. Rev. B* **77**, 224115 (2008).
- [37] J. P. Perdew, A. Ruzsinszky, G. I. Csonka, O. A. Vydrov, G. E. Scuseria, L. A. Constantin, X. Zhou, and K. Burke, Restoring the Density-Gradient Expansion for Exchange in Solids and Surfaces, *Phys. Rev. Lett.* **100**, 136406 (2008).
- [38] See Supplemental Material at <http://link.aps.org/supplemental/10.1103/PhysRevB.97.174103> for the structural information of the predicted ground-state B_{9,5}Se, given by [B₁₂(Se-Se)]_{0.34}[B₁₂(B-Se)]_{0.33}[B₁₂(Se-B)]_{0.33} (Fig. 5). The internal atomic coordinates, volume, and cell shape are relaxed.
- [39] A. Togo and I. Tanaka, First principles phonon calculations in material science, *Scr. Mater.* **108**, 1 (2015).
- [40] A. Togo, F. Oba, and I. Tanaka, First-principles calculations of the ferroelastic transition between rutile-type and CaCl₂-type SiO₂ at high pressures, *Phys. Rev. B* **78**, 134106 (2008).
- [41] K. Parlinski, Z. Q. Li, and Y. Kawazoe, First-Principles Determination of the Soft Mode in Cubic ZrO₂, *Phys. Rev. Lett.* **78**, 4063 (1997).
- [42] A. van de Walle and M. Asta, Self-driven lattice-model Monte Carlo simulations of alloy thermodynamics properties and phase diagrams, *Model. Simul. Mater. Sci.* **10**, 521 (2002).
- [43] H. C. Longuet-Higgins and M. de V. Roberts, The electronic structure of an icosahedron of boron atoms, *Proc. R. Soc. A* **230**, 110 (1955).
- [44] H. Zhang, S. Yao, and M. Widom, Predicted phase diagram of boron-carbon-nitrogen, *Phys. Rev. B* **93**, 144107 (2016).